Feng *et al. Energy Mater.* **2025**, *5*, 500112
DOI: 10.20517/energymater.2025.04

Energy Materials

Article

Open Access

Check for updates

Maskless formation of patterned leather-based conductive electrode for human-computer interaction application

Haihang Feng[2,3,#], Yu Xiao[4,#], Wenjie Yang[3], Haitong Yang[2,3], Ruihao Zhou[3], Jincheng Lin[3], Mingcen Weng[2,*], Huamin Chen[1,3,6,*], Yun Xu[1,5,6]

[1]Institute of Semiconductors, Chinese Academy of Sciences, Beijing 100083, China.
[2]Institute of Biology and Chemistry, Fujian University of Technology, Fuzhou 350118, Fujian, China.
[3]Fujian Key Laboratory of Functional Marine Sensing Materials, College of Materials and Chemical Engineering, Minjiang University, Fuzhou 350108, Fujian, China.
[4]College of Physics and Electronic Information Engineering, Minjiang University, Fuzhou 350108, Fujian, China.
[5]College of Materials Science and Opto-Electronic Technology, University of Chinese Academy of Sciences, Beijing 100049, China.
[6]Beijing Key Laboratory of Inorganic Stretchable and Flexible Information Technology, Beijing 100083, China.
[#]Authors contributed equally.

***Correspondence to:** Assoc. Prof. Huamin Chen, Institute of Semiconductors, Chinese Academy of Sciences, No. A35, Qinghua East Road, Haidian District, Beijing 100083, China. E-mail: chenhuamin@semi.ac.cn; Assoc. Prof. Mingcen Weng, Institute of Biology and Chemistry, Fujian University of Technology, No. 69, Xuefu South Road, Shangjie Town, Minhou County, Fuzhou 350118, Fujian, China. E-mail: wengmc@fjut.edu.cn

How to cite this article: Feng, H.; Xiao, Y.; Yang, W.; Yang, H.; Zhou, R.; Lin, J.; Weng, M.; Chen, H.; Xu, Y. Maskless formation of patterned leather-based conductive electrode for human-computer interaction application. *Energy Mater.* **2025**, *5*, 500112. https://dx.doi.org/10.20517/energymater.2025.04

Received: 8 Jan 2025 **First Decision:** 14 Mar 2025 **Revised:** 24 Mar 2025 **Accepted:** 15 Apr 2025 **Published:** 22 May 2025

Academic Editor: Yizhong Huang **Copy Editor:** Fangling Lan **Production Editor:** Fangling Lan

Abstract

Leather-based materials have found extensive use in the development of flexible sensing devices, energy harvesting, storage systems, and flexible circuits owing to their high biocompatibility, good breathability, comfort during wear, and robust mechanical properties. However, with the rapid evolution of flexible electronics, traditional fabrication methods for leather-based devices fail to fulfill the demands for high integration and practicality. In this work, an innovative fabrication method combining laser direct writing and inkjet printing technologies has been developed to prepare a self-powered triboelectric sensor array for human-computer interaction applications. This method offers significant advantages, including mask-free fabrication, high resolution, and fast processing. The resulting MXene/graphene/leather (MG/leather) electrode exhibits a narrow width (400 μm), high conductivity (1.46 S mm^{-1}), strong adhesion strength (2.63 MPa), and high tensile strength (7.65 MPa). The MG/leather-based

TENG achieves a maximum output voltage of 167.5 V, a current density of 1.1 mA m^{-2}, a transferred charge of 144.5 μC m^{-2}, a power density of 6.25 μW/cm^2, and remarkable mechanical stability exceeding 10,000 cycles. Furthermore, the self-powered triboelectric sensor array, mounted on human skin, enables the effective manipulation of cartoon games in a computer program, highlighting its potential applications in the metaverse. This work advances the industrialization and commercialization of flexible electronics.

Keywords: Leather, triboelectric nanogenerator, flexible electronics, MXene, laser-induced graphene, printing

INTRODUCTION

Flexible and wearable devices have garnered considerable attention owing to their ability to enhance daily life, particularly in human-computer interaction (HCI), health monitoring, and metaverse application[1-5]. Various types of flexible sensors attached to the skin or clothing collect visual, auditory, olfactory, taste, and tactile information for big data analysis[6-10]. As the foundational unit of flexible electronics, flexible electrodes play a critical role in device performance and industrialization. Typically comprising conductive nanomaterials and flexible polymer substrates such as polydimethylsiloxane (PDMS)[11], polyimide (PI)[12,13], Ecoflex[14,15], and styrene-butadiene-styrene (SBS)[16,17], these electrodes have seen significant advancements in recent years. However, beyond flexibility and mechanical properties, considerations such as breathability, processability, and adaptability are equally vital owing to the prolonged interaction between wearable devices and human skin.

Leather, as a natural polymer, offers formidable advantages over traditional flexible substrates[18-20]. It is abundant, biocompatible, breathable, comfortable, flexible, and mechanically strong[21-23], making it an ideal carrier for diverse flexible electronics. Various conductive materials have been incorporated into leather to form composite electrodes, including MXene[24], silver nanowires[25], graphene oxides[23], carbon nanotubes[26] and poly(3,4-ethylenedioxythiophene)-poly(styrenesulfonate) (PEDOT:PSS)[27]. Leather-derived materials have found extensive use in the development of flexible sensors[28,29], energy conversion and storage devices[30,31], and flexible circuits[32,33]. However, with the rapid evolution of flexible electronics, traditional fabrication methods for leather-based devices fail to meet the requirements for high integration and practicality. Therefore, developing high-precision and patterned processing methods has become a pressing need.

Conventional processing methods include vacuum-assisted filtration[34,35], spray coating[36], printing[28,37] and laser direct writing[38,39]. For instance, Zhang *et al.* fabricated a patterned triboelectric nanogenerator (TENG) array by vacuum filtration of MXene on leather for human-machine interface applications[40]. Ma *et al.* created silver nanowire-decorated leather with panda patterns via direct painting for Joule heating, electromagnetic interference shielding, and piezoresistive sensing[41]. In addition, Zhang *et al.* developed a flexible tactile sensor array by screen-printing carbon paste onto leather surfaces for robotic interactive skin[42]. While vacuum filtration and spraying are simple and cost-effective, they require pattern templates, severely limiting their patterning capabilities. Although printing offers patterning capabilities, it is time-consuming to optimize the inks' viscoelasticity. Notably, Wang *et al.* fabricated a 3 × 3 flexible strain sensor array on leather using laser direct writing[38]. This technique is simple and efficient, but it only carbonizes the leather into carbon materials, restricting conductivity and versatility.

In this work, a self-powered triboelectric sensor array is successfully fabricated on leather for HCI applications via a novel fabrication strategy. This strategy, which combines laser direct writing and inkjet printing, offers high resolution and fast processing. More importantly, the as-prepared MXene/graphene/

leather (MG/leather) electrode, fabricated without mask assistance, exhibits high conductivity and adhesion strength. The MG/leather electrode features a width of 400 μm, conductivity of 1.46 S mm^{-1}, adhesion strength of 2.63 MPa, and tensile strength of 7.65 MPa. The MG/leather-derived TENG achieves a maximum output voltage of 167.5 V, current density of 1.1 mA m^{-2}, transferred charge of 144.5 μC m^{-2}, and power density of 6.25 μW cm^{-2}. This maskless, high-resolution strategy, coupled with superior triboelectric sensing performance, enables complex HCI applications. The self-powered triboelectric sensor array, mounted on human skin, effectively manipulates cartoon games in a computer program, showcasing potential applications in the metaverse. This work advances the industrialization and commercialization of flexible electronics.

EXPERIMENTAL

Preparation of single/few-layer MXene ($Ti_3C_2T_x$) nanosheets

MXene ($Ti_3C_2T_x$) was synthesized via an etching process utilizing a lithium fluoride powder (LiF, Aladdin) and hydrochloric acid (HCl, Aladdin) solution. Firstly, the MXene etchant was formulated by dissolving 4.6 g of LiF powder in a 9 M HCl solution with stirring for 5 min at room temperature. Subsequently, 2 g MAX phase (Ti_3AlC_2, supplied by Jilin 11 Technology Co., Ltd.) was separated into three aliquots, and one portion was incorporated into the LiF/HCl solution every 3 min with continuous stirring. The above solution was hermetically sealed in a reactor and continuously stirred magnetically in a water bath maintained at 80 °C for 72 h. The resulting mixture was thoroughly washed three times with 0.1 M HCl, followed by several centrifugations with distilled water until the pH reached 7. The resulting precipitate was dried at 60 °C, ground into a powder, and dispersed in dimethyl sulfoxide (DMSO) with stirring for 18 h. The suspension was centrifuged at 10,000 rpm, and the precipitate was collected. Lastly, the inkjet printing ink was formulated by adding deionized water and subjecting the mixture to ultrasonic shaking. The ink concentration was calibrated to 30 mg/mL.

Fabrication of MG/leather electrode

The leather substrate was processed using a laser engraving system (30 W CO_2 laser engraving system, Universal Laser Systems, Scottsdale, AZ, USA) to create laser-induced graphene (LIG) electrodes on the surface of leather fibers. The patterns of the LIG electrodes were regulated by parameters including geometric patterns, power intensity, scanning velocity, and material thickness. In this investigation, a laser engraving system of 27 W and a speed of 60% were employed, with line widths reaching up to 400 μm. The patterned LIG/leather substrate was then processed using an inkjet printing apparatus (flexible electronic printer, Scientific 3, Shanghai Mifang Electronics Technology Co., Ltd.) for MXene inkjet printing. Detailed fabrication parameters are listed in Supplementary Table 1. Following a simple heating process, the MG/leather electrode was obtained.

Construction of MG/leather-based TENG and its applications

The MG/leather electrode functioned as both the bottom electrode and triboelectric layer, while conductive silver tape and Ecoflex (Dow Corning) constituted the top electrode and the triboelectric layer, respectively. A contact-separation TENG structure was constructed. The performance of the TENG was tested by mounting it on both sides of a linear electromechanical actuator (R-LSP1, China) and applying force. The effective area of the MG/leather-based TENG used for testing was 2 × 2 cm^2. For wireless remote control of computer games, push-button triboelectric sensors were prepared on the surface of leather fibers by combining laser writing and inkjet printing techniques. The HCI control enabled various movements of a chick in the computer game. This work optimizes the number of interfaces in haptic display arrays, presenting significant potential for the development of large-area, multi-unit sensing systems.

Characterization

The surface topography of the LIG electrodes, 2D MXene films, and MG/leather was analyzed via scanning electron microscopy (SEM, SU8000, Hitachi, Tokyo, Japan) and transmission electron microscopy (TEM, Talos F200S and JEM-F200). X-ray diffraction (XRD) spectra were recorded with a Bruker analytical instrument via Cu $K\alpha_1$ radiation (λ = 0.154 nm) over a 3°-70° range at a scanning speed of 10°/min. The tensile properties of the samples were evaluated utilizing a universal testing machine (Instron 3343). Electrical conductivity was evaluated with a four-point probe testing system (FT-345, ROOKO, Ningbo, China), utilizing a probe spacing of 2.35 mm and a probe radius of 0.5 mm. Compressive and tensile forces were applied via a linear electromechanical actuator (R-LSP1, China), and the electrical output performance of the TENG was measured using an electrometer meter (Keithley 6517B, Tektronix, Inc., Beaverton, OR, USA).

RESULTS AND DISCUSSION

The preparation process of the MG/leather electrode is depicted in Figure 1A. First, MXene ($Ti_3C_2T_x$) nanosheets were synthesized using a milder etching technique, as described in our prior research[40]. Multilayer $Ti_3C_2T_x$ was initially prepared by etching MAX phase Ti_3AlC_2 powders with HCl/LiF to generate HF *in situ*. Two-dimensional (2D) aqueous-phase dispersions of $Ti_3C_2T_x$ nanosheets were then obtained by treating the multilayer MXene with DMSO, followed by centrifugation at 10,000 rpm. Stabilized MXene inks were formed by adding deionized water and subjecting the mixture to ultrasonic vibration, with the ink concentration adjusted to 30 mg/mL. Patterned leather-based triboelectric sensors were fabricated by combining laser printing and inkjet printing. The leather fiber surface was irradiated with a laser printer to form a conductive LIG pattern. MXene patterns were subsequently printed onto the LIG/leather substrate to create the conductive MG/leather electrode. This novel method fabricates highly conductive leather-based electrodes without mask assistance and offers advantages such as high resolution and fast processing. As shown in Figure 1B, the interlocking layer design drew inspiration from the symbiotic relationship between a beehive and honey, where the perforated honeycomb structure holds honey securely in place. Similarly, the LIG layer functions as a porous framework, providing microchannels that interlock the MXene film with the flexible substrate. This design enhances interfacial adhesion between the electrode and substrate while restricting the migration of MXene ink. Large-scale patterns such as a complex school logo pattern "MJU" can also be achieved, as shown in Figure 1C. The MG electrode achieves a line width of 400 μm. Optical photographs of the LIG/leather and MXene films are provided in Supplementary Figure 1A and B. The successful fabrication of MG/leather composites was confirmed by XRD analysis [Figure 1D]. The XRD spectra of both MG/leather and MXene exhibit a broader (002) peak near 2θ = 6.11°, indicating that MXene nanosheets were effectively embedded into the pore-like structure of the LIG/leather.

The structural and functional characterization of MXene/leather, LIG/leather, and MG/leather is shown in Figure 2. To evaluate the mechanical and electrical properties of the MG electrodes, cross-sectional SEM images of the MG films were analyzed. As shown in Figure 2A, the middle layer comprises an interlocking structure of porous LIG filled with MXene nanosheets, while the upper multilayered structure represents the MXene layer, and the intricate fibers below represent the leather layer. This unique structure significantly enhances interfacial strength while maintaining high electrical conductivity. The SEM images of the MG/leather surface [Figure 2B] reveal a rough texture, attributed to the distribution of fibers, which facilitates the adhesion of the MXene film. The energy-dispersive X-ray spectroscopy (EDS) spectra and elemental mapping [Figure 2C] confirm the uniform distribution of titanium (Ti), carbon (C), oxygen (O), and fluorine (F) on the MG surface. The cross-sectional SEM imaging of the MXene layered structure [Figure 2D] shows clear delamination of the layered MXene structure, while the TEM micrograph in the inset highlights the good single-crystal quality of the nanosheets. The surface topography of the LIG framework was analyzed via SEM [Figure 2E], which reveals its porous structure. An enlarged SEM image

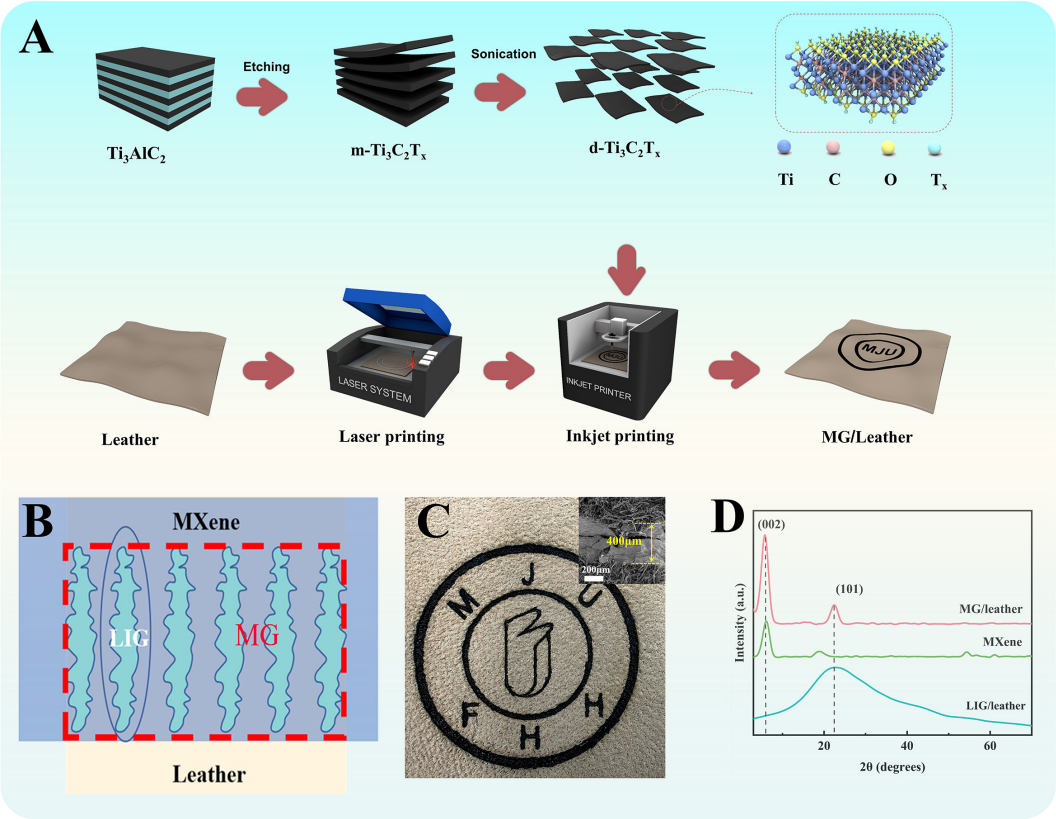

Figure 1. (A) Preparation strategy of the MG/leather composite; (B) schematic diagram of the interlocking structure formation at the LIG/MXene interface; (C) patterned school logo "MJU" electrodes (inset shows a line width of 400 μm); (D) XRD spectrum of the LIG/leather, MXene, and MG/leather films.

[Figure 2F] shows that the pore size is approximately 1 μm, providing ample space for the infiltration of MXene nanosheets. The adhesion strength of various electrodes on the leather substrate was measured using a standard test procedure [Figure 2G]. The interfacial bonding strengths of LIG, MG, and MXene films were 0.73, 2.63, and 0.38 MPa, respectively. As a reference, reduced graphene oxide (rGO)/MXene was coated onto a leather substrate, achieving an adhesion strength of only 0.3 MPa, highlighting the superior performance of the MG structure. The mechanical properties of leather, LIG/leather, and MG/leather were also evaluated. As shown in Figure 2H, the tensile strength of MG/leather is 7.65 MPa, significantly exceeding that of leather (6.3 MPa) and LIG/leather. The fracture strain of MG/leather reaches 70.6%, attributed to the tight wrapping of collagen fiber bundles by the MXene nanosheets and the extensive hydrogen bonding interactions within the porous structure. The LIG interlocking layer enhances adhesion and mechanical strength, demonstrating the efficacy of this strategy. Considering the changes in conductivity of the MG electrode during deformation, we tested its resistance cycling under different contact forces, with the results shown in Supplementary Figure 2A. The resistance exhibits a decreasing trend as the force is applied, and the greater the contact force, the more pronounced the change becomes. Figure 2I compares the conductivity of various leather-based composite electrode materials. The MXene/Leather was fabricated by directly patterning on the leather substrate using an inkjet printing system. The LIG electrode on leather exhibits negligible conductivity, whereas the MG/leather composite achieves a conductivity of 1.46 S mm^{-1}, comparable to that of MXene/leather.

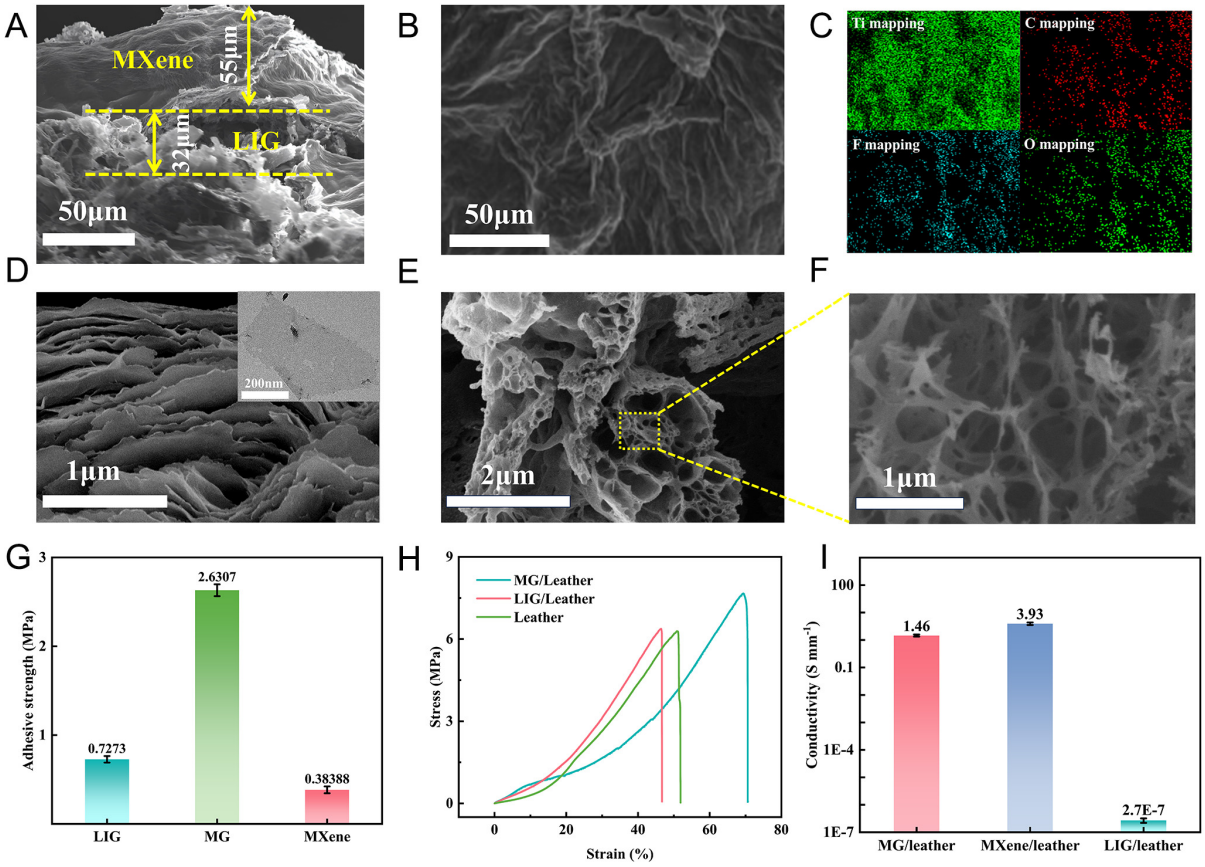

Figure 2. (A) Cross-sectional SEM imaging of the MG/leather film; (B) superficial SEM of the MG/leather film; (C) elemental mapping of Ti, C, O, and F on the MG/leather surface; (D) Cross-sectional SEM imaging of the MXene layered structure (inset: TEM analysis); (E) SEM imaging of the LIG layer; (F) high-resolution SEM of the LIG layer; (G) adhesion strength of electrodes on various leather bases; (H) strain-stress curves of leather, LIG/leather, and MG/leather; (I) comparison of conductivity among LIG/leather, MG/leather, and MXene films.

TENGs typically consist of two materials with differing electronegativity: electropositive and electronegative materials. The electropositive material loses electrons during contact, while the electronegative material attracts electrons. In this study, a contact-separated TENG was assembled using MG/leather as the negative electrode and triboelectric layer, with Ecoflex and Ag serving as the other friction layer and electrode, respectively. The operational principle of the MG/leather-based TENG is depicted in Figure 3A. In the equilibrium state [Figure 3A(i)], there is no potential difference between the two electrodes, and no charge transfer occurs. When external force is applied [Figure 3A(ii)], opposite charges are induced on the surfaces of the leather and Ecoflex triboelectric layers. However, the potential difference remains negligible, preventing electron flow between the two electrodes. Upon release of the external force [Figure 3A(iii)], a potential difference is created, driving electron flow from the MG electrode to the Ag electrode. At this point [Figure 3A(iv)], the potential difference and transferred charge reach their maximum values. When the external force is reapplied [Figure 3A(v)], the potential difference reverses, inducing electron flow back to the MG terminal from the Ag terminal. This periodic contact-separation process, driven by a linear motor [Figure 3B], generates a continuous low-frequency alternating current (AC). Optical image and its machine control system have been shown in Supplementary Figure 2B and C. It can be seen that there is a sensor in the base to record the real-time pressure, and that the sensor can be calibrated through a computer interface to directly control the pressure value. Finite element method (FEM) simulations were conducted to analyze potential changes under open-circuit conditions [Figure 3C-F]. Under open-circuit conditions,

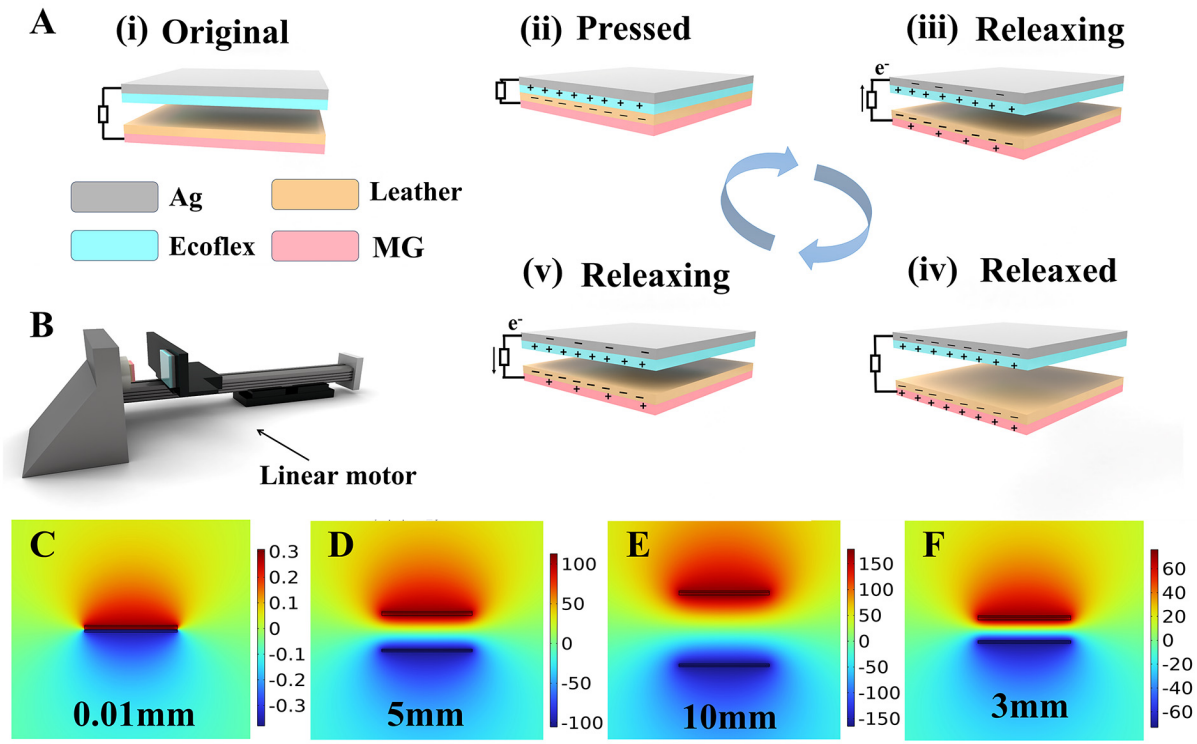

Figure 3. (A) Schematic diagram of the working mechanism of the MG/leather-TENG; (B) schematic of the linear motor system used for TENG performance testing; finite element modeling (FEM) of potential distribution between two electrodes: (C) in contact; (D) separated by 5 mm after contact; (E) at a maximum separation distance of 10 mm; (F) 3 mm before contact.

no current is generated between the electrodes, and the output voltage rises linearly with the separation distance between the MG/leather and Ecoflex layers. As the separation distance rises from 0.01 to 10 mm, the potential difference escalates from 0.3 to 170 V.

To assess the output efficiency of TENGs based on MG/leather, LIG/leather, and MXene/leather, different electrodes on a uniform substrate were prepared and tested. A linear electromechanical actuator was utilized to generate cyclic contact-separation motion, allowing for adjustments in frequency and contact force. The effective contact area in the experiment was 2 × 2 cm^2 under a 10 N force at a frequency of 1 Hz. The output voltages of the different electrode-based TENGs are presented in Figure 4A. The MG/leather-based TENG exhibited the highest output voltage of 88.3 V, while the output voltages of the LIG/leather and MXene/leather-based TENGs were 3.9 and 88.3 V, respectively. The output current density and transferred charge density followed the same trend, as shown in Figure 4B and C. The MG/leather-based TENG demonstrated optimal output efficiency, a charge density of 85.13 μC m^{-2} and exhibiting a current density of 0.54 mA m^{-2}. These values represent significant improvements, with enhancements of 2,200% and 275% compared to the output performance of the LIG/leather and MXene/leather TENGs, respectively. This enhanced performance can be ascribed to the inverse proportionality between maximum output performance and the thickness of the insulating layer. The carbonization of the leather fiber surface during irradiation reduces its thickness, enhancing the triboelectric effect. The lower output performance of the LIG/leather-TENG is due to its inherently low conductivity. To further assess the mechanical energy harvesting capability, the effects of varying contact forces (at a constant frequency of 1 Hz) on the output performance were investigated, as shown in Figure 4D-F. The output voltage, current density, and charge density of the MG/leather-based TENG increased with the applied contact force, reaching maximum values of 167.5 V, 1.1 mA m^{-2}, and

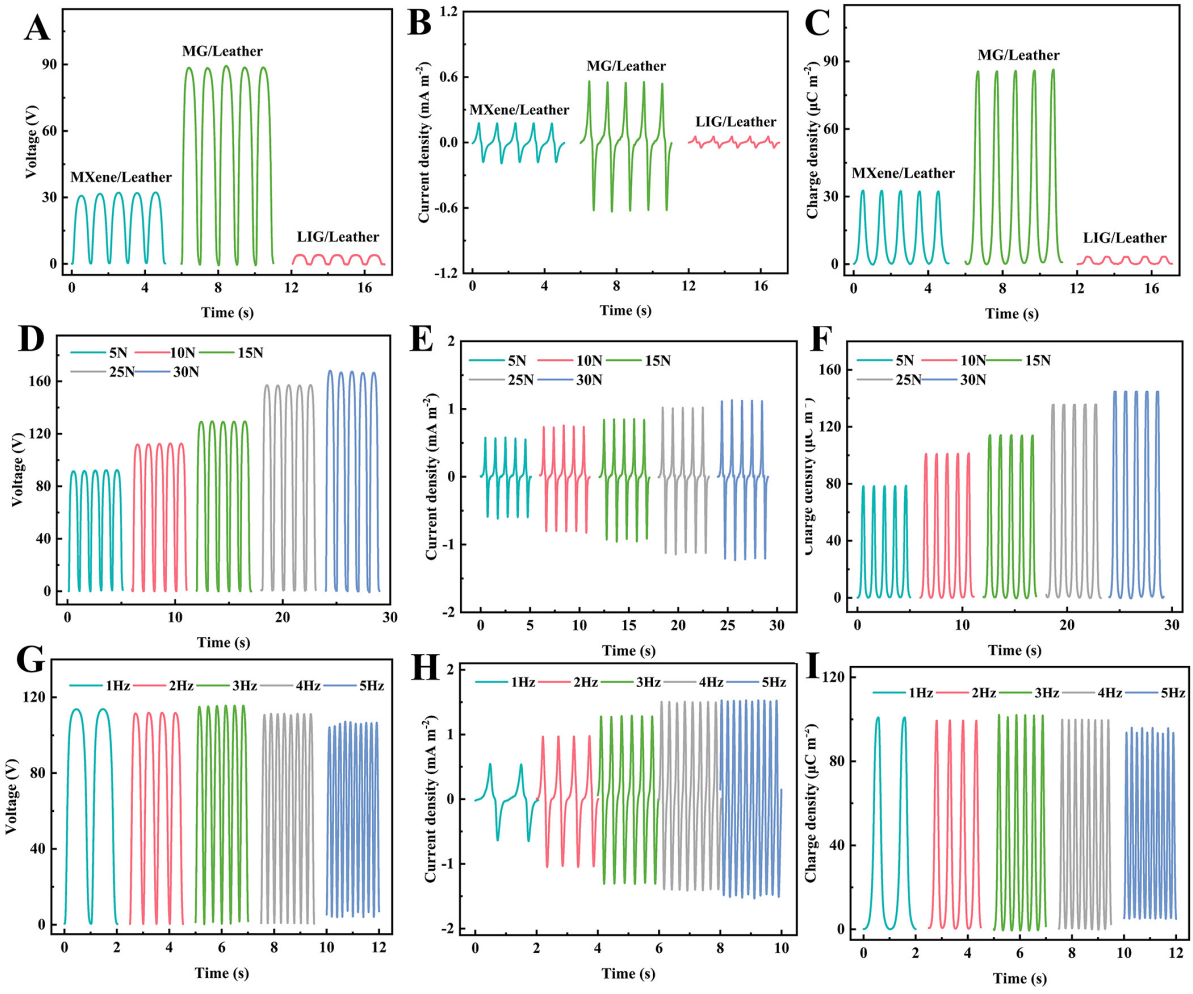

Figure 4. (A) Output voltage of MXene/leather, MG/leather, and LIG/leather-based TENGs; (B) output current density; (C) transferred charge density; (D) output voltage of the MG/leather-based TENG under different external contact forces; (E) output current density; (F) transferred charge density; (G) output voltage of the MG/leather-based TENG at frequencies ranging from 1 to 5 Hz; (H) output current density; (I) transferred charge density.

144.5 μC m^{-2}, respectively, at a contact force of 30 N. These results demonstrate that the MG/leather electrode maintains its structural integrity under higher forces. Additionally, the performance of the MG/leather electrode as both the triboelectric layer and the electrode was tested under varying contact forces (at a constant frequency of 1 Hz) [Supplementary Figure 3]. The output performance of the MG/leather-based TENG was also evaluated at frequencies ranging from 1 to 5 Hz, as shown in Figure 4G-I. Under an external compressive force of 10 N, the output current density increased with frequency, reaching a saturation value of 1.53 mA m^{-2} at 5 Hz. In contrast, the output voltage and transferred charge density exhibited stability across varying frequencies. The invariance of output voltage and transferred charge density with frequency is explained by the creation of triboelectric charges during the contact-separation process, which remains constant regardless of frequency. However, the frequency influences the electron flow rate, which exhibits a linear correlation with the output current density.

The output power and energy delivery capacity of the MG/leather-based TENG are crucial for practical implementation. A self-charging circuit based on the TENG was constructed, as shown in Figure 5A. A

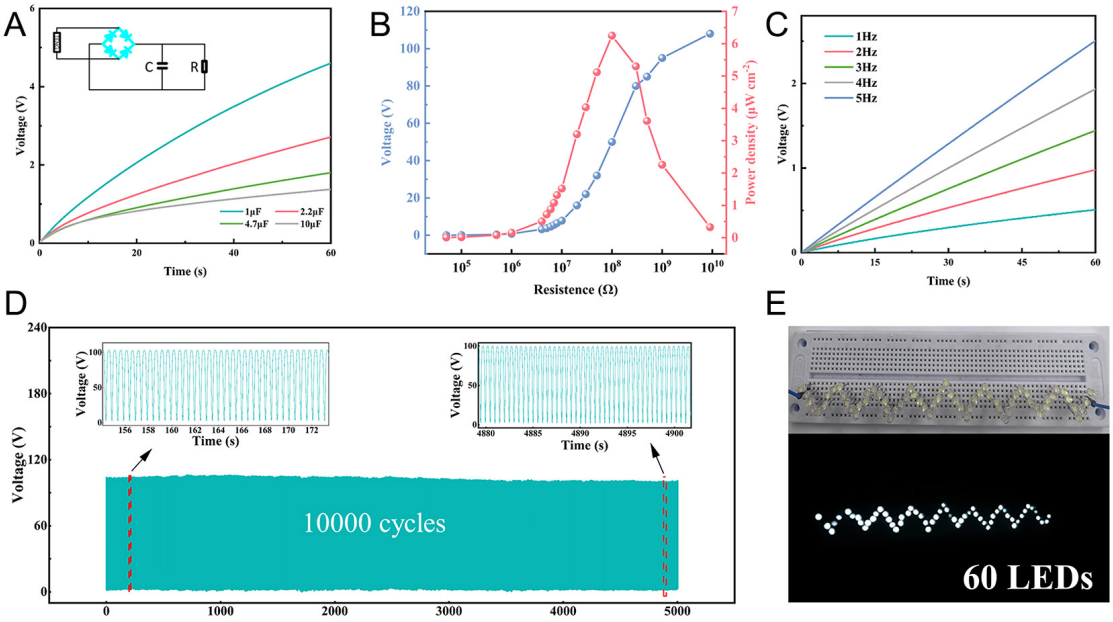

Figure 5. (A) Charging profiles of capacitors with different capacitances, along with the operational circuitry of the TENG-based self-charging energy system; (B) output voltage and power density of the MG/leather-based TENG as a function of external load resistance; (C) charging curves of a 10 μF capacitor powered by the TENG at different frequencies; (D) stability test of the MG/leather-based TENG under a contact force of 10 N at 2 Hz; (E) optical photograph of 60 LEDs illuminated by the MG/leather-based TENG.

bridge rectifier was employed to transform the AC produced by the MG/leather-TENG into direct current (DC), which was subsequently stored in a capacitor to power low-energy electronic devices.

The charging capability of the MG/leather-TENG at 1 Hz was tested using capacitors with varying capacitances (1, 2.2, 4.7, and 10 μF) [Figure 5A]. The findings demonstrate that the MG/leather-based TENG is capable of charging a 1 μF capacitor to 4.7 V in 60 seconds. Even a 10 μF capacitor was charged to 1.7 V within 60 s, sufficient to power certain microelectronic devices. To evaluate the power output and voltage of the MG/leather-TENG under varying load conditions, resistors were employed as external loads, as shown in Figure 5B. The output power density P is calculated by the equation $P = U^2/RS$, where U is the output voltage, R is the load resistance, and S is the effective area of the device. As the resistance increased from 50 kΩ to 10 GΩ, the output voltage also increased, eventually stabilizing at approximately 108 V. At a load resistance of 100 MΩ, the maximum output power density reached 6.25 μW cm^{-2}. The charging profiles of a capacitor with a capacitance of 10 μF at varying frequencies are illustrated in Figure 5C. These curves demonstrate that the MG/leather-based TENG delivers high efficiency and stable power output within a short duration. Durability tests were performed to evaluate the reliability of the TENG in real-world scenarios, as depicted in Figure 5D. The output voltage of the TENG was measured under a contact force of 10 N at a frequency of 2 Hz for approximately 5,000 s. The voltage remained stable at around 100 V, and even after 10,000 cycles, no significant performance degradation was observed. This validates the long-term operational reliability of the device. The MG/leather-based TENG efficiently converts mechanical energy into low-frequency electrical power, demonstrating its capability to power up to 60 commercial light-emitting diodes (LEDs) [Figure 5E]. As a versatile energy source for self-sustaining systems, the MG/leather-based TENG exhibits excellent output performance and stability, highlighting its potential as a reliable and flexible energy source. A comparative performance evaluation of the proposed maskless fabrication method and other conventional techniques for different leather-based composites is summarized in Supplementary Table 2, providing an intuitive overview of their efficiencies. Leather-based electrodes

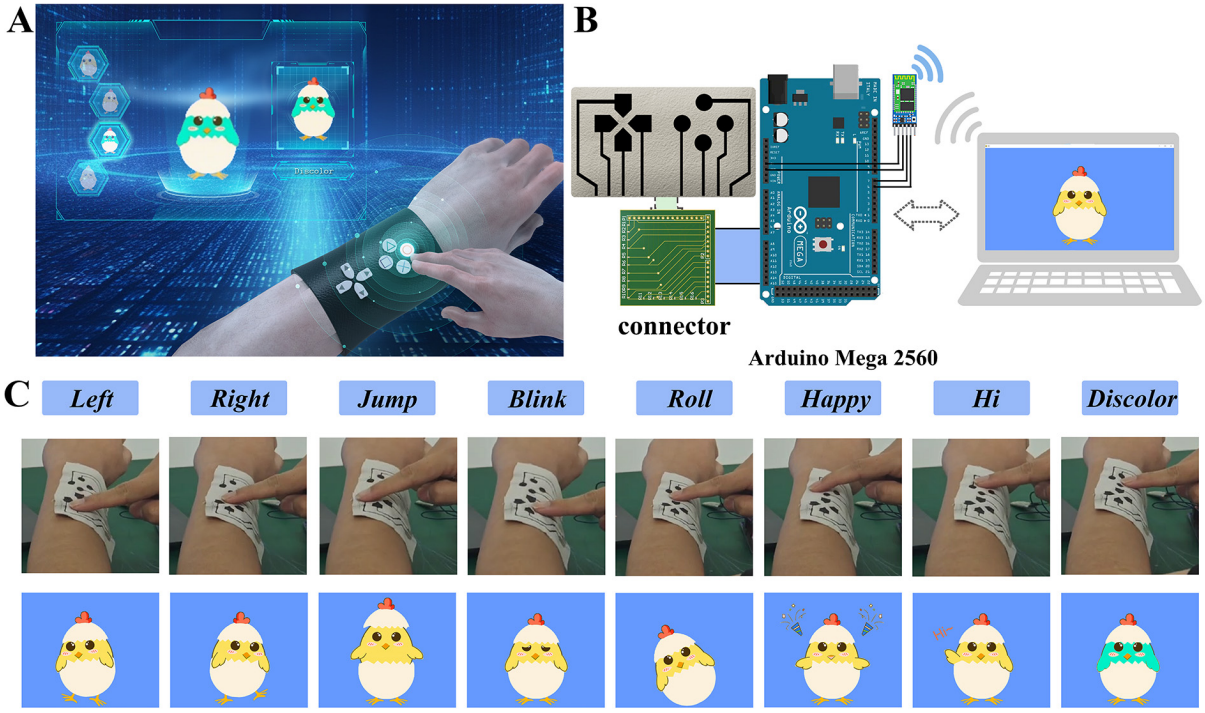

Figure 6. (A) Schematic of the wireless MG/leather-TENG control signal transmitter; (B) computerized receiver setup; (C) button mapping corresponding to the operations of the chicklet.

offer significant advantages over conventional flexible electronics, including superior breathability, cost-effectiveness, and eco-friendliness, while addressing key challenges in HMI applications. Their excellent biocompatibility ensures safe skin contact, and their durability and mechanical properties enable long-term use. Additionally, leather's natural texture allows for seamless integration into wearable devices, enhancing user comfort and acceptance.

In addition to serving as a stable power source for external microelectronic devices, the MG/leather electrode can be patterned for human-machine interaction (HCI). Using a novel fabrication strategy, an MG/leather-based triboelectric sensor was developed, as illustrated in Supplementary Figure 4A. The schematic diagram of the self-powered HCI system is depicted in Figure 6A. This system can be mounted on the skin to wirelessly control computer games. Voltage values were recorded by interacting with sensor units, and cross-coding was employed to minimize signal interference at the mapping ports, enabling efficient and fast signal extraction. An Arduino Mega 2560 motherboard was used to capture and analyze these signals. The sensor array includes Bluetooth connectivity and an energy storage unit [Figure 6B]. The keyboard array serves as a complete control terminal, interfacing with a computer via Bluetooth to form a functional game operating system. In a simple demonstration game, different keys were used to control a virtual chick, with available actions such as walking, jumping, blinking, wiggling, celebrating, greeting, and changing colors [Figure 6C]. The waveforms corresponding to each action are shown in Supplementary Figure 4B, and the chick's movements can be viewed in detail in Supplementary Video 1. The MG/leather-based triboelectric sensor enables effective manipulation of simple games in a computer program, demonstrating potential applications in intelligent gaming and offering insights for the advancement of next-generation flexible wearable technologies.

CONCLUSIONS

In summary, a novel fabrication method combining laser direct writing and inkjet printing technologies has been developed to prepare a self-powered triboelectric sensor array for HCI applications. This method offers significant advantages, including mask-free fabrication, high resolution, and fast processing. The resulting MG/leather electrode exhibits a narrow width (400 μm), high conductivity (1.46 S mm^{-1}), strong adhesion strength (2.63 MPa), and high tensile strength (7.65 MPa). The MG/leather-based TENG achieves a maximum output voltage of 167.5 V, a current density of 1.1 mA m^{-2}, a transferred charge of 144.5 μC m^{-2}, a power density of 6.25 μW cm^{-2}, and remarkable mechanical stability exceeding 10,000 cycles. Furthermore, the self-powered triboelectric sensor array, mounted on human skin, enables the effective manipulation of cartoon games in a computer program, highlighting its potential applications in the metaverse. This work advances the industrialization and commercialization of flexible electronics.

DECLARATIONS

Authors' contributions

Investigation, original draft writing: Feng, H.
Investigation, visualization: Xiao, Y.
Investigation: Yang, W.
Formal analysis: Yang, H.
Data curation: Zhou, R.
Software: Lin, J.
Writing-review & editing, Funding acquisition: Weng, M.
Supervision, Funding acquisition: Chen, H.
Visualization, Writing-review & editing: Xu, Y.

Availability of data and materials

The datasets generated or analyzed during this study are available from the corresponding authors upon reasonable request.

Financial support and sponsorship

This work was supported by the National Natural Science Foundation of China (Nos. 52201043, 52103138), the Natural Science Foundation of Fujian (No. 2024J011310), and Fashu Charity Foundation of Minjiang University (MFK24024).

Conflicts of interest

All authors declared that there are no conflicts of interest.

Ethical approval and consent to participate

Not applicable.

Consent for publication

Not applicable.

REFERENCES

1. Wang, Y.; Liang, J.; Yu, J.; et al. Multiscale haptic interfaces for metaverse. *Device* **2024**, *2*, 100326. DOI
2. Chung, H. U.; Kim, B. H.; Lee, J. Y.; et al. Binodal, wireless epidermal electronic systems with in-sensor analytics for neonatal

intensive care. *Science* **2019**, 363. DOI PubMed PMC
3. Zhao, C.; Park, J.; Root, S. E.; Bao, Z. Skin-inspired soft bioelectronic materials, devices and systems. *Nat. Rev. Bioeng.* **2024**, *2*, 671-90. DOI
4. Zhang, K.; Wu, Y.; Lu, J.; et al. Biocompatible salt-enhanced thin porous humidity sensor for human interaction sensing. *Sens. Actuat. B. Chem.* **2025**, *425*, 136907. DOI
5. Rehman, H. M. M. U.; Prasanna, A. P. S.; Rehman, M. M.; Khan, M.; Kim, S.; Kim, W. Y. Edible rice paper-based multifunctional humidity sensor powered by triboelectricity. *Sustain. Mater. Technol.* **2023**, *36*, e00596. DOI
6. Liu, Y.; Park, W.; Yiu, C. K.; et al. Miniaturized, portable gustation interfaces for VR/AR/MR. *Proc. Natl. Acad. Sci. USA.* **2024**, *121*, e2412116121. DOI PubMed PMC
7. Zhu, Q. B.; Li, B.; Yang, D. D.; et al. A flexible ultrasensitive optoelectronic sensor array for neuromorphic vision systems. *Nat. Commun.* **2021**, *12*, 1798. DOI PubMed PMC
8. Niu, H.; Li, H.; Gao, S.; et al. Perception-to-cognition tactile sensing based on artificial-intelligence-motivated human full-skin bionic electronic skin. *Adv. Mater.* **2022**, *34*, e2202622. DOI
9. Deng, Y.; Zhao, M.; Ma, Y.; et al. A flexible and biomimetic olfactory synapse with gasotransmitter-mediated plasticity. *Adv. Funct. Mater.* **2023**, *33*, 2214139. DOI
10. Yang, Q.; Jin, W.; Zhang, Q.; et al. Mixed-modality speech recognition and interaction using a wearable artificial throat. *Nat. Mach. Intell.* **2023**, *5*, 169-80. DOI
11. Wang, Z.; Xia, X.; Zhu, M.; et al. Rational assembly of liquid metal/elastomer lattice conductors for high-performance and strain-invariant stretchable electronics. *Adv. Funct. Mater.* **2022**, *32*, 2108336. DOI
12. Rehman, M. M.; Samad, Y. A.; Gul, J. Z.; et al. 2D materials-memristive devices nexus: from status quo to Impending applications. *Prog. Mater. Sci.* **2025**, *152*, 101471. DOI
13. Lin, J.; Peng, Z.; Liu, Y.; et al. Laser-induced porous graphene films from commercial polymers. *Nat. Commun.* **2014**, *5*, 5714. DOI PubMed PMC
14. Xiao, J.; Zhan, B.; He, M.; et al. Mechanically robust and thermal insulating nanofiber elastomer for hydrophobic, corrosion-resistant, and flexible multifunctional electromagnetic wave absorbers. *Adv. Funct. Mater.* **2025**, *35*, 2419266. DOI
15. Kim, S.; Kang, J.; Lee, I.; et al. An intrinsically stretchable multi-biochemical sensor for sweat analysis using photo-patternable ecoflex. *NPJ. Flex. Electron.* **2023**, *7*, 268. DOI
16. Choi, S.; Han, S. I.; Jung, D.; et al. Highly conductive, stretchable and biocompatible Ag-Au core-sheath nanowire composite for wearable and implantable bioelectronics. *Nat. Nanotechnol.* **2018**, *13*, 1048-56. DOI
17. Zhong, D.; Wu, C.; Jiang, Y.; et al. High-speed and large-scale intrinsically stretchable integrated circuits. *Nature* **2024**, *627*, 313-20. DOI
18. Fan, Z.; Sang, M.; Gong, X.; Leung, K. C.; Xuan, S. From natural leather to intelligent wearable nanocomposite: design and application. *Soft. Sci.* **2024**, *4*, 11. DOI
19. Zhu, J.; Liu, Y.; Xie, R.; et al. A breathable, designable and flexible leather-heater used in wearable thermotherapy. *Sci. China. Technol. Sci.* **2024**, *67*, 2125-32. DOI
20. Lyu, B.; Ouyang, Y.; Gao, D.; Wan, X.; Bao, X. Multilevel and flexible physical unclonable functions for high-end leather products or packaging. *Small* **2025**, *21*, e2408574. DOI
21. Basak, S.; Shakyawar, D. B.; Samanta, K. K.; et al. Cellulose-protein blended sustainable biodegradable flexible composite: a step towards a leather alternative. *Cellulose* **2023**, *30*, 11087-112. DOI
22. Xie, R.; Hou, S.; Chen, Y.; et al. Leather-based strain sensor with hierarchical structure for motion monitoring. *Adv. Mater. Technol.* **2019**, *4*, 1900442. DOI
23. Zhang, P.; Zhang, X.; Teng, M.; et al. Leather-based shoe soles for real-time gait recognition and automatic remote assistance using machine learning. *ACS. Appl. Mater. Interfaces.* **2024**, *16*, 62803-16. DOI
24. Fan, Z.; Lu, L.; Sang, M.; et al. Wearable safeguarding leather composite with excellent sensing, thermal management, and electromagnetic interference shielding. *Adv. Sci.* **2023**, *10*, e2302412. DOI PubMed PMC
25. Li, J.; Cui, M.; Wen, J.; et al. Leather-like hierarchical porous composites with outstanding electromagnetic interference shielding effectiveness and durability. *Compos. B. Eng.* **2021**, *225*, 109272. DOI
26. Wang, P.; Feng, J.; Bai, Y.; et al. Zirconium ion ligand cross-linked carbon nanotubes and leather collagen fibers for flexible, stable, and highly efficient underwater sensors. *Chem. Eng. J.* **2024**, *480*, 148201. DOI
27. Zong, Y.; Tan, S.; Ma, J. Flame-retardant PEDOT:PSS/LDHs/leather flexible strain sensor for human motion detection. *Macromol. Rapid. Commun.* **2022**, *43*, e2100873. DOI
28. Xie, R.; Du, Q.; Zou, B.; et al. Wearable leather-based electronics for respiration monitoring. *ACS. Appl. Bio. Mater.* **2019**, *2*, 1427-31. DOI
29. Zhou, T.; Hu, S.; Ji, W.; et al. An integrated leather-based fluid transport wearable sweat device for electrolyte balance monitoring. *J. Mater. Chem. C.* **2024**, *12*, 9363-71. DOI
30. Fan, J.; Yuan, M.; Wang, L.; Xia, Q.; Zheng, H.; Zhou, A. MXene supported by cotton fabric as electrode layer of triboelectric nanogenerators for flexible sensors. *Nano. Energy.* **2023**, *105*, 107973. DOI
31. Lyu, B.; Li, H.; Gao, D.; Li, N.; Zheng, C. High output performance leather-based triboelectric nanogenerator by tuning charge trapping and transport. *Nano. Energy.* **2024**, *132*, 110342. DOI

32. Kim, D. H.; Kim, Y. S.; Wu, J.; et al. Ultrathin silicon circuits with strain-isolation layers and mesh layouts for high-performance electronics on fabric, vinyl, leather, and paper. *Adv. Mater.* **2009**, *21*, 3703-7. DOI
33. Pandey, R.; Biswas, A. K.; Chakraborty, U. Non-conventional leather substrate based high isolation wideband MIMO antenna for body-centric applications. *Int. J. Electron. Commun.* **2023**, *170*, 154871. DOI
34. Zhou, J.; Chen, H.; Zhou, P.; et al. $Ti_3C_2T_x$ MXene nanosheet-functionalized leathers for versatile wearable electronics. *ACS. Appl. Nano. Mater.* **2023**, *6*, 18150-64. DOI
35. Zou, B.; Chen, Y.; Liu, Y.; et al. Repurposed leather with sensing capabilities for multifunctional electronic skin. *Adv. Sci.* **2019**, *6*, 1801283. DOI PubMed PMC
36. Wilson, N. H.; Ragothaman, M.; Palanisamy, T. Bimetallic copper-iron oxide nanoparticle-coated leathers for lighting applications. *ACS. Appl. Nano. Mater.* **2021**, *4*, 4055-69. DOI
37. Xie, R.; Zhu, J.; Wu, H.; et al. 3D-conductive pathway written on leather for highly sensitive and durable electronic whisker. *J. Mater. Chem. C.* **2020**, *8*, 9748-54. DOI
38. Wang, Z.; Chen, B.; Sun, S.; Pan, L.; Gao, Y. Maskless formation of conductive carbon layer on leather for highly sensitive flexible strain sensors. *Adv. Elect. Mater.* **2020**, *6*, 2000549. DOI
39. Yang, D.; Nam, H. K.; Le, T. D.; et al. Multimodal E-textile enabled by one-step maskless patterning of femtosecond-laser-induced graphene on nonwoven, knit, and woven textiles. *ACS. Nano.* **2023**, *17*, 18893-904. DOI
40. Zhang, S.; Xiao, Y.; Chen, H.; et al. Flexible triboelectric tactile sensor based on a robust MXene/leather film for human-machine interaction. *ACS. Appl. Mater. Interfaces.* **2023**, *15*, 13802-12. DOI
41. Ma, Z.; Xiang, X.; Shao, L.; Zhang, Y.; Gu, J. Multifunctional wearable silver nanowire decorated leather nanocomposites for joule heating, electromagnetic interference shielding and piezoresistive sensing. *Angew. Chem. Int. Ed.* **2022**, *61*, e202200705. DOI
42. Zhang, B.; Meng, W.; Cheng, G.; et al. Leather-based printed tactile sensor array for robotic interactive skin. *Nano. Energy.* **2024**, *132*, 110379. DOI